BILINGUAL PUBLISHING GROUP

Journal of Atmospheric Science Research

https://journals.bilpubgroup.com/index.php/jasr

ARTICLE

Convective Available Potential Energy and Convective Inhibition in ERA-Interim Reanalysis during the AMMA SOP Campaign

Cyrille Meukaleuni [1,2*] **, *Cyrille A. Mezoue*** [3] **, *Eric Efon*** [4] **, *Sinclair Zebaze*** [5] **, *André Lenouo*** [2*] **, *David Monkam*** [2] **, *Desmond Manatsa*** [6]

[1]*Department of Physics, The University Institute of the Coast, Douala P.O Box 3001, Cameroon*

[2]*Department of Physics, Faculty of Science, University of Douala, Douala P.O Box 24157, Cameroon*

[3]*Department of Physics, National Higher Polytechnic School of Douala, University of Douala, Douala P.O Box 24157, Cameroon*

[4]*Department of Physics, Faculty of Science, University of Bamenda, Bambili P.O. Box 39, Cameroon*

[5]*Indiana University Bloomington: Bloomington, Indiana, Bloomington, IN 47405-7000, USA*

[6]*Department of Geography, Faculty of Letter, Bindura University of Science Education, Bindura P. Bag 1020, Zimbabwe*

ABSTRACT

A statistical analysis of Convective Inhibition (CIN) and Convective Available Potential Energy (CAPE) is conducted using a six-hourly ERA-Interim dataset for the summer of 2006 over West Africa as part of the African Monsoon Multidisciplinary Analyses (AMMA) SOP3 Campaign. This study analyses the trends and empirical orthogonal functions (EOF) of CAPE and CIN, along with the summer variability of CAPE and CIN with precipitation. CAPE exhibits its maximum over the continent around 14°N, while CIN peaks over the ocean. The variance of the main EOF is about 42% and its amplitude is low in the equatorial zone and slightly higher in the Sahelian regions. The variance of the second EOF is 16.4% and shows its maximum towards the south of Gambia. The significance of the trends of the pairs (first and second) of CAPE and CIN with rainfall is explored through the canonical correlation analysis (CCA) of these three parameters. The first and

*CORRESPONDING AUTHOR:

Cyrille Meukaleuni, Department of Physics, The University Institute of the Coast, Douala P.O Box 3001, Cameroon; Department of Physics, Faculty of Science, University of Douala, Douala P.O Box 24157, Cameroon; Email: meukaleuni@yahoo.fr; André Lenouo, Faculty of Science, Department of Physics, University of Douala, Douala P.O Box 24157, Cameroon; Email: lenouo@yahoo.fr

ARTICLE INFO

Received: 21 November 2024 | Revised: 7 January 2025 | Accepted: 11 January 2025 | Published Online: 15 January 2025
DOI: https://doi.org/10.30564/jasr.v8i1.7841

CITATION

Meukaleuni, C., Mezoue, C.A., Efon, E., et al., 2025. Convective Available Potential Energy and Convective Inhibition in ERA-Interim Reanalysis during the AMMA SOP Campaign. Journal of Atmospheric Science Research. 8(1): 1–12. DOI: https://doi.org/10.30564/jasr.v8i1.7841

second pairs of CCA show a correlation of around 68% and 60%, respectively, with 12.2 and 10.8 degrees of freedom. The correlation coefficient at the 95% confidence level is 0.21 for the first CCA pairs and 0.65 for the second CCA pairs. In the Sahelian and Sudanese regions, the variance is approximately 78% and 73% respectively, primarily driven by the first CCA pair. The Guinea and wet equatorial areas are influenced by the second CCA pair, where the explained regional variance exceeds 60%.

Keywords: CAPE; CIN; West Africa; Era-Interim

1. Introduction

Convection is one of the means of heat transmission by air circulation, which leads to vertical atmospheric motions, driven by either dynamic or thermodynamic factors operating simultaneously. The thermal structure of moisture and the divergence field of atmospheric circulation are respectively the thermodynamic and dynamic characteristic elements of the atmosphere. However, it is difficult to distinguish the contributions of each of these two factors in convection. It should be noted that convection can be an important element of the Earth's climate and is particularly important in the formation of cumulus and cumulonimbus clouds. Conversely, the development of cumulus and cumulonimbus clouds is primarily influenced by the general atmospheric circulation (orientation and force of the wind), affecting precipitation patterns [1].

The activities and health of the population in West Africa (WA) are directly impacted by weather phenomena such as cloud cover, heavy rainfall, storms, wind gusts, and others. Through in-situ measurements, various research centers aimed at studying atmospheric stability, which led to improved understanding and prediction of convective events. These studies utilize stability indices that reflect atmospheric conditions at specific levels [1–4]. These indices, derived from temperature differences at key atmospheric levels, have been used in the development of forecast models for atmospheric convection [5], as well as for predicting convective precipitation and severe weather systems [6–9]. Additionally, they have been incorporated into general circulation models for the parameterization of cumulus clouds [10].

Besides, when less dense air rises, it is accompanied by the downward movement of a thicker, colder, and heavier air volume. The lowering of the center of the system leads to the transformation of gravitational potential energy into kinetic energy since the mass of the descending air exceeds that of the ascending air. For an air parcel to participate in convection and reach a certain level, it must possess sufficient energy. Convective Inhibition (CIN), or convective braking, represents the energy required to provide a parcel of moist air with enough energy to initiate free convection. When energy is supplied to an air parcel to overcome CIN at a particular atmospheric level, the air is lifted convectively, increasing CAPE.

CAPE and CIN are stability indices that do not rely on a single atmospheric level, which makes them popular for assessing the convective potential of the atmosphere. Thus, two quantities are calculated by integrating the vertical atmospheric profile. Meukaleuni et al. [11] through the study of seasonal CAPE, show high CAPE values between 12° and 16°N, peaking in summer due to increased relative humidity from monsoon winds, using ERA-Interim over the WA region for 35 years from 1979 to 2014. Their analysis included seasonal averages, variances, and trends. They also found that spectral analysis in the latitude 10°–20°N and longitude 20°W–30°E region, where CAPE was maximum near the ITCZ's summer position, revealed significant 3–5 day power linked to tropical deep convection from African easterly waves. Wahiduzzaman et al. [12] explored how CAPE, temperature, and humidity affect thunderstorm patterns in Bangladesh using an EOF approach. They found that thunderstorms increased in areas where they were less common and decreased where they were more frequent. These authors also show a downward/upward trend in CAPE in winter/monsoon and on an annual scale. Thus, just before the monsoon, the frequency of storms was strongly correlated with air humidity, and CAPE, as opposed to the increase in temperature.

To improve the understanding of the processes influencing weather conditions at different spatial and temporal scales, the AMMA SOP program organized, in 2006, a special campaign to collect field data, which led to the identification of the African Easterly Waves (AEWs)—waves with

wavelengths of 2000 to 4000 km, lasting 3 to 5 days, and moving in the west at a speed of 8 ms-1 —as key drivers of the variability of the WA monsoon. The research also highlighted the crucial role of the Intertropical Convergence Zone (ITCZ) in establishing the WAM and identified AEWs as major weather systems within this phenomenon, as illustrated in **Figure 1**[13–15]. Numerous studies[16–22] have demonstrated the significance of AEWs in the formation of Mesoscale Convective Systems (MCS), which are crucial for rainfall in West Africa, accounting for around 90% of the annual rainfall in the Sahel[23].

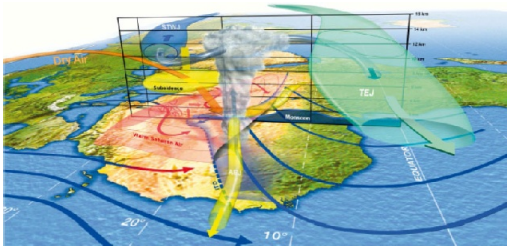

Figure 1. Representation of the WA monsoon in three-dimensional. Intertropical Discontinuity (ITD), African Easterly Jet (AEJ), Subtropical Westerly Jet (STWJ). The oscillation of the yellow tube of the AEJ around 600–700 hPa represents an African Easterly Wave (AEW) (from Lafore et al., 2010[13]).

Variations of CAPE are primarily influenced by changes in the atmospheric boundary layer[24, 25]. To further explore this, Ye et al.[10] analyzed temperature and specific humidity at 2 meters. Romero et al.[26] created a 30-year climatology of CAPE and CIN using ERA-40 data from the ECMWF over Europe. Brooks et al.[8] developed a global CAPE climatology based on seven years of NCEP (National Centre for Environmental Prediction) reanalysis data. Trapp et al.[27] examined the climatology of CAPE for both present-day and future scenarios using simulations from various coupled atmosphere-ocean models in the United States. Riemann-Campe[28] expanded the global climatology analysis for CAPE and CIN, using 44 years of the ERA-40 dataset to provide seasonal ensemble means, second moments, and trend analysis.

This work also correlated CAPE and CIN with convective precipitation by using ERA-40 reanalysis data from 1979–2001 and ECHAM5/MPI-OM model data from 1979–2099, analyzing trends, memory, and changes in a warmer climate. However, a statistical analysis characterizing the climatology of the WA region is still needed. This study presents an analysis of CAPE and CIN based on the ERA-Interim dataset from the summer of 2006 over WA, collected during the AMMA SOP3 Campaign, which included extensive soundings in the region[29]. We aim to analyze the climatology of CAPE and CIN by using EOF and to investigate their relationship with rainfall through CCA.

The paper is structured as follows: the data, study area, and methods are presented in Section 2; Section 3 discusses the climatology of CAPE and CIN; and Section 4 offers conclusions and perspectives.

2. Data and Method

2.1. Data

We used here the data coming from the ERA-Interim global atmospheric reanalysis, which covers the period from 1979 to the present provided by ECMWF[30]. The analysis is also based on the 2006 AMMA field experiment, during which a lot of soundings were conducted in West Africa[29]. Additionally, we used the Global Precipitation Climatology Project (GPCP) monthly precipitation dataset, version 2[31–33], for the period from June to September 2006, with a 2.5 by 2.5-degree global grid, provided by the National Oceanic and Atmospheric Administration (NOAA).

2.2. Brief Presentation of CAPE and CIN

CAPE represents the energy needed to lift an air parcel adiabatically from the Level of Free Convection (LFC), known as the cloud base, to the Level of Neutral Buoyancy (LNB), known as the cloud top. CAPE is the difference in virtual temperature between an idealized rising air parcel (Tvp) and the surrounding environment (Tve). The parcel continues to rise freely between the base and top of the cloud as long as its temperature remains higher than that of the environment. CAPE is calculated using Equation (1) below:

$$\mathrm{CAPE} = \int_{\mathrm{LFC}}^{\mathrm{LNB}} g \left(\frac{T_{\mathrm{Vp}} - T_{\mathrm{Ve}}}{T_{\mathrm{Ve}}} \right) \mathrm{dz} \qquad (1)$$

Where g represents the acceleration of gravity and z represents altitude. Experimentally, it has been observed that high CAPE values do not always correlate with strong convection.

CIN is a numerical measure that indicates the energy needed to prevent an air parcel from rising from the surface (SFC) to the Level of Free Convection (LFC). It represents the energy required to overcome the buoyancy exerted by

the environment on the air parcel between the surface and the LFC. CIN, which is expressed as a negative energy value, is calculated using Equation (2) below:

$$\text{CIN} = \int_{\text{SFC}}^{\text{LFC}} g \left(\frac{T_{\text{Ve}} - T_{\text{Vp}}}{T_{\text{Ve}}} \right) \text{dz} \tag{2}$$

As a result of the density of an air parcel is greater (due to its lower temperature) compared to the surrounding air, it experiences downward acceleration due to the negative buoyancy exerted on it. As a result, this layer of air becomes warmer and more stable relative to the layers above and below it.

2.3. Statistic Analysis

The EOF is a multivariate statistical method used to reduce a climate dataset with a large number of (Kx1) vectors x to a smaller set of (Mx1) vectors u, which is the linear combinations of the original dataset that capture most of the information, x's. Typically, anomalies $x' = x - \bar{x}$ are used to compute the elements of these new vectors, known as principal components (PCs). Each principal component u_m, where m = 1, 2, 3, 4, …of u represents a linear combination of x' with the most significant variance and is uncorrelated with the principal components (PCs) of lower indices with the first component having the most significant variance. These principal components are derived by projecting the data vector x' to the mth eigenvector e_m of the covariance matrix of x, [S], as shown by Equation (3) below[34].

$$u_m = e_m^T x' = \sum e_{k,m} x'_k \quad m = 1, 2, \ldots, M \tag{3}$$

Where e_m^T denotes the transpose of the eigenvector $e_{m.}$, each of the M eigenvectors has one element corresponding to each of the K variables x_k.

The Mann-Kendall trend test is used to investigate potential trends in a time series. For instance, for a time series x_i, where i ranges from 1 to n, the statistic for this test, τ, is calculated by Equation (4) below[34].

$$\tau = \sum_{i=1}^{n-1} \text{sgn}\left(x_{i+1} - x_i\right) \tag{4}$$

The sign function, $\text{sgn}(x_{i+1} - x_i)$, indicates the direction of change in the time series x_i, assigning values of –1 for decreases, +1 for increases, and 0 for no change. We employed this test to detect trends in CAPE and CIN, as well as analyze seasonal trends. Linear regression estimated the trend magnitudes. Only trends exceeding the 95% significance level were considered.

Canonical Correlation Analysis (CCA) was used to compare two transformed variable groups, examining if they represent the same physical phenomenon. CCA seeks pairs of weights that maximize correlations between new variables created by projecting original data onto multivariate sets. Canonical vectors for variables x and y are derived from eigenvectors and eigenvalues a_m and b_m using Equations (5) and (6)[34]:

$$a_m = [S_{x,x}]^{\frac{-1}{2}} e_m \tag{5}$$

$$b_m = [S_{y,y}]^{\frac{-1}{2}} f_m \tag{6}$$

Where e_m is the eigenvector associated with the variable x, and f_m is the eigenvector associated with the variable y for (m = 1, …, M). The (I x I) matrix $[S_{x,x}]$ represents the covariance matrix for the I variables in x, while the (J x J) matrix $[S_{y,y}]$ represents the covariance matrix for the J variables in y. In this study, the CCA of CAPE, and CiN with rainfall is computed for the corresponding EOFs.

3. Results and Discussions

3.1. Overview of Climatology during the AMMA SOP CAMPAIGN

Figure 2 illustrates the spatial variations in precipitation from 0 to 25°N and between 20°W and 30°E of the period JJAS 2006. In June (**Figure 2a**), the maximum rainfall is concentrated along the equatorial coast of West Africa. This peak shifts northward towards the Sahara region in July (**Figure 2b**) and August (**Figure 2c**). By September (**Figure 2d**), the area of maximum precipitation stretches from the 0 to 15°N, confined within the region (0°N–15°N lat, 10°E–15°W lon). The figure also reveals a back-and-forth of the peak precipitation between the Guinea coast and the Sahel during the summer, resulting in two rainy seasons per year in the southern region and one in the northern region.

Cool, moist air from the Gulf of Guinea is brought over the continent where it meets warm, dry air. This produces an 'energy exchange between the land surface and the ocean and helps to sustain the surface monsoon flow in the southwest of WA. These observations put in light the influence of the ITCZ on rainfall in the region by confirming that the maximum rainfall over WA shifts northward dur-

ing the summer. As described by Sultan and Janicot [35], the ITCZ is the meeting point of two air masses: the dry, warm Saharan Air Layer (SAL) associated with the Saharan Heat Low (SHL), and the cooler, moist monsoon flow issue of the subtropical South Atlantic. This convergence is marked by convective activity within the Hadley cells, often resulting in large cumulonimbus formations [36].

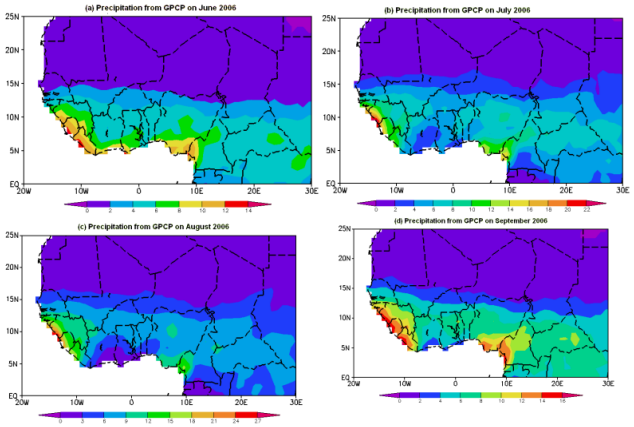

Figure 2. Mean precipitation over WA from GPCP reanalysis during June (**a**), July (**b**), August (**c**), and September (**d**) 2006. The WA countries' contours are shown with a dash and the interval of rainfall is 2 mm/day.

Figure 3 demonstrates the first three principal components (PCs) of rainfall over WA during JJAS 2006. The PC1 time series (**Figure 3a**) has negative a phase from June to mid-July, shifting to a positive phase with a brief return to the negative phase in the last days of September. PC2 (**Figure 3b**) and PC3 (**Figure 3c**) show significant fluctuations throughout June to September. PC1 accounts for approximately 44% of the total variance, PC2 around 12%, and PC3 over 7.5%.

3.2. CAPE and CIN Climatology and Trends

Figures 4 and **5** show the climatological averages of CAPE (**Figure 4**) and CIN **(Figure 5**) from June to September 2006. The maximum CAPE occurs around the AEJ axis (15°N) in July (**Figure 4b**), though its values decrease before increasing and shifting northward in August (**Figure 4c**). The highest CAPE is observed in northern Nigeria in June (**Figure 4a**), in eastern Mali in August **(Figure 4c**), and it moves southward to southern Chad by September (**Figure 4d**). This migration pattern of CAPE mirrors the movement of the ITCZ over WA during rainy season.

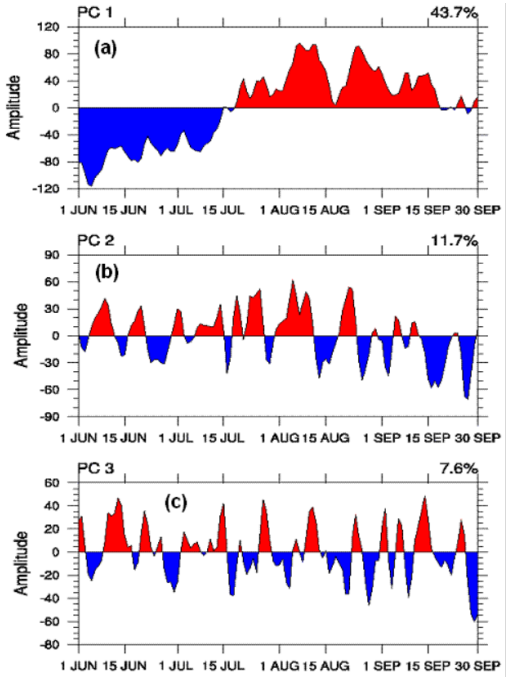

Figure 3. First three PC of the rainfall over WA during the period JJAS 2006. PC1 (**a**), (**b**) PC2, and (**c**) PC3. The values on the top right corner of each pattern represent its percentage of the total variance.

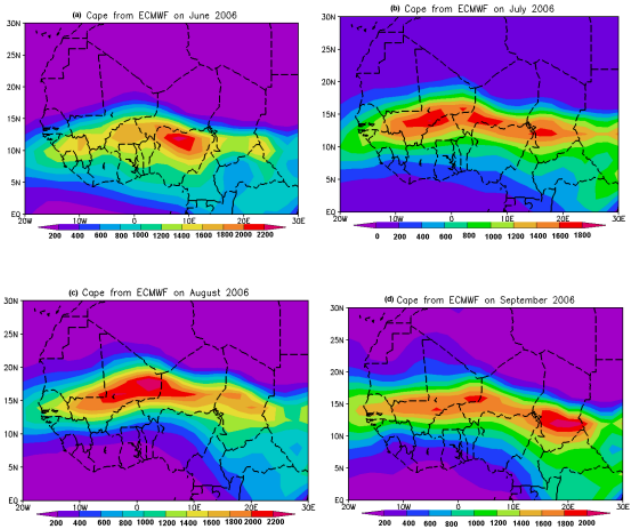

Figure 4. Mean CAPE in J/kg over WA from ECMWF reanalysis during the months of (**a**) June, (**b**) July, (**c**) August, and (**d**) September 2006. The WA countries' contours are shown with a dash and the interval of CAPE is 200 J/kg.

The average CIN activity is primarily concentrated over the ocean near the Senegalese coast. Maximum CIN is located around 15°N in June (**Figure 5a**), moving northward in July (**Figure 5b**) and August (**Figure 5c**) to 20°N, where its values decrease from 650 J/kg to 400 J/kg in September (**Figure 5d**). The area of maximum CIN coincides with

the regions where various storms formed during the SOP campaign[37]. This result shows that African easterly waves (AEW) developing over the Atlantic Ocean may be related to the CIN, while the ITCZ would be related to the CAPE, influencing convection in this region.

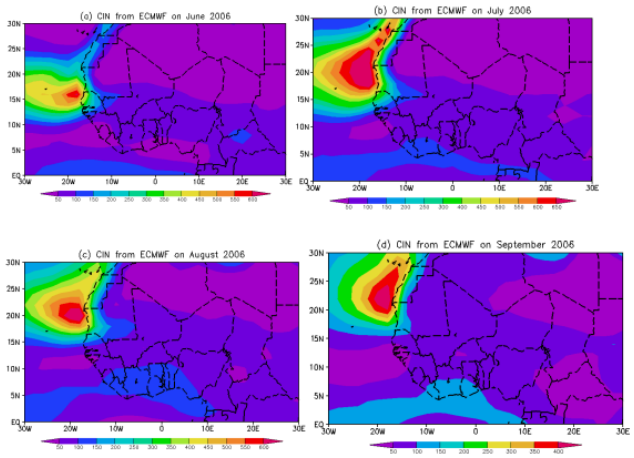

Figure 5. Mean CIN in J/kg over West Africa from ECMWF re-analysis during the months of (**a**) June, (**b**) July, (**c**) August, and (**d**) September 2006.

Figure 6 presents the first three EOFs of CAPE and CIN during the 2006 rainy season. The percentage variance values corresponding to each EOF are shown in the upper panel. The first EOF (PC1) of CAPE accounts for approximately 42% of the total variance, its slightly higher values in the north and lower values along the wet region. The second EOF, accounting for 16.4% of the variance, has its maximum towards the south of Gambia. The third EOF (PC3) shows a contrast between maximum and minimum values around 15°N. Additionally, the figure shows that the first EOF of CIN is about 44% of the total variance, and the second explains over 12%.

Figure 7 illustrates the first three PCs of CAPE and CIN over WA, derived from the Era-Interim dataset from JJAS 2006. The PC1 time series of CAPE had a negative phase from June to mid-July, then it shifted to a positive phase that continued until the end of September. This component accounts for approximately 52% of total variance. The PC2 of CAPE was mainly in a negative phase during the first half of June and from August 15th through the end of September. The PC3 of CAPE showed a negative phase in June and August, and a positive phase in all months of July-September. PC2 and PC3 are for roughly 12% and over 6% of total variance, respectively. For CIN, the PC1 time series has a negative phase in June and during the second half of August-September. It was in a positive phase from July to the first half of August, and again in the first half of September. The PC2 of CIN remained mostly positive from June to the first half of August and turned negative for the remainder of the period. The PC3 of CIN also has a negative phase from June to mid-July and the first half of September, while being in a positive phase for the rest of the period. These three principal components of CIN (PC1, PC2, and PC3) account for approximately 55%, 15%, and 8% of the total variance, respectively.

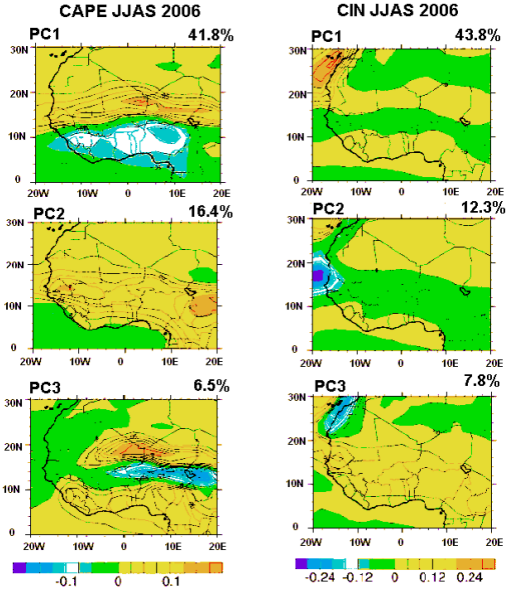

Figure 6. First three EOF of CAPE (on **left**) and CIN (on **right**) during JJAS 2006 over WA from Era-Interim. The values on the top right corner of each pattern represent its percentage of the total variance. The country limits are shown by a contour.

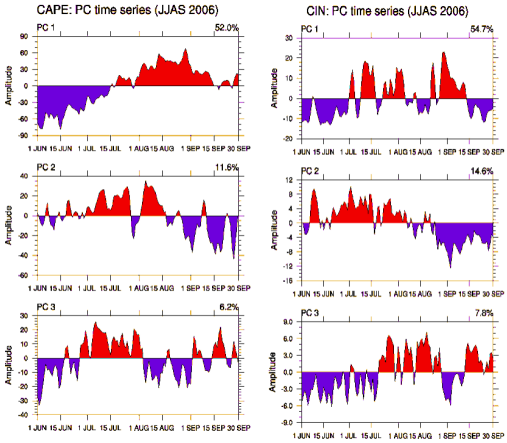

Figure 7. First three PC of CAPE (on **left**) and CIN (on **right**) during JJAS 2006 over WA from Era-Interim. The values on the top right corner of each pattern represent its percentage of the total variance.

There is a substantial similarity between the PC1 time series of CAPE (**Figure 7**) and the rainfall data from GPCP (**Figure 3**). The PC2 time series of CAPE generally opposes the phase of PC1 from June 1 (day 1) to July 15 (day 45) and from August 15 (day 76) to September 30 (day 122), while being in phase between July 15 and August 15. Both PCs exhibit a positive phase from June 15 (day 15) to August 15 (day 76) and a negative phase during the remaining days of the JJAS period. The similar variance values in the PC1, PC2, and PC3 time series of CAPE and CIN suggest that either parameter can characterize convection dispersion in this region. We also found that the time series of rainfall PC1 (PC2) in Fig 3 significantly correlates with the time series of CAPE PC1 (PC2) in **Figure 7** at the 95% confidence level.

The trend magnitudes of CAPE (**Figure 8**) and CIN (**Figure 9**) are represented in **Figures 8** and **9** respectively at the significance level exceeds 95%. Data points recorded every 6 hours over West Africa during the period JJAS 2006 were used to determine these trends. Significant CAPE trends are observed around the AEJ axis (15°N). Trend magnitudes, initially measured in J/kg per 6 hours, were converted to J/kg per decade for comparison with previous studies. In June (**Figure 8a**), trend magnitudes vary from about -300 J/kg to approximately 800 J/kg per decade, with a notable increase of around 800 J/kg per decade occurring in the Central African Republic. In July (**Figure 8b**), trends are between -450 J/kg and 150 J/kg per decade, with negative trends remaining near 15°N. The most significant increase in the CAPE, about 400 J/kg per decade, is seen in the Sahara region over central Chad during August (**Figure 8c**), while the most significant decrease, around 450 J/kg per decade, is found in the same area in June, shifting eastward to southern Mali in September (**Figure 8d**). Similar trend changes were also observed by Meukaleuni et al.[11]. They found that significant trends occurred over shorter periods due to a change in trend direction after 1978. This change resulted in a net increase of 200 to 600 J/kg per decade from June to September (JJS) 1958–2001. This shift in trend direction was also noted in central Africa, Malaysia, and Venezuela when considering the southern hemisphere in 1978. The study also suggested that trends in CAPE are driven by trends in near-surface specific humidity.

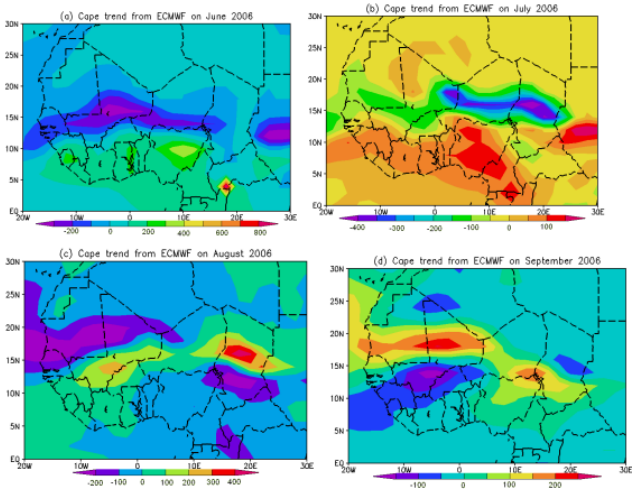

Figure 8. Trends of the CAPE in J/kg per decade which are significant at the 95% level over WA during (**a**) June, (**b**) July, (**c**) August, and (**d**) September of the year 2006. The WA countries' contours are shown by a black dashed line.

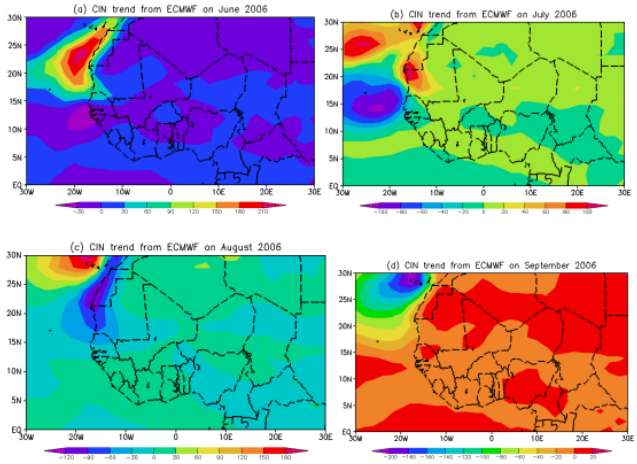

Figure 9. Trends of the CIN in J/kg per decade which are significant at the 95% level over WA during (**a**) June, (**b**) July, (**c**) August, and (**d**) September of the year 2006. The WA countries' contours are shown by a black dashed line.

CIN trends generally occur in regions where maximum CIN was observed, as shown in **Figure 5**. However, the trends in CIN exhibit opposite signs from June to August compared to September. Compared to the trends reported by Riemann-Campe et al.[38] in central Africa from 1979 to 2001, an increase in CAPE is noted, while CIN is decreasing. The important decrease, about 190 J/kg per decade, is found over the Atlantic Ocean, which is similar to the 200 J/kg per decade decrease observed in September 2006 (**Figure 9d**). The most significant increase, around 210 J/kg per decade, is seen along the coast of Morocco in June 2006 (**Figure 9a**). During the AMMA SOP3 campaign, CIN trends ranged

from approximately –200 to 210 J/kg per decade. Due to the generally low values of the CIN, the observed change in sign is less pronounced for this parameter. As noted in Riemann-Campe et al. [38], this sign change is most distinct in Mexico and the USA during June to August (JJA), in central Africa throughout the year, and in Brazil during JJA and September to November (SON).

3.3. Correlation of CAPE and CIN with Precipitation

The climatic zones over the West Africa region, defined by four sub-regions identified using Cluster Analysis (CA) on July, August, and September (JAS) rainfall anomalies from 1961–1998, are presented in **Figure 10** [39]. The first sub-region (GI), located between 17.5°N and 30°N, primarily encompasses the Sahara. The second sub-region (GII), located between 17.5°N and 7.5°N and defined as the West Sudan sub-region, is centered on Chad, with a relatively uniform extension westward towards Mauritania and eastward to include the northern Central African Republic. The third sub-region (GIII), located between latitudes 7.5°N and 5°N and stretching from 7.5°W on the west coast to 7.5°E, is centered on the Ivory Coast and extends to cover parts of Nigeria., it is. The fourth sub-region (GIV), known as the Guinea Coast region and covering the wet areas in Central Africa, is bounded by latitudes 5°N and 0°N, and between 7.5°E to 25°E. For simplicity, the Sahara and Sudan regions are confined between 15°W and 30°E. This regional classification was used to analyze six static stability measures over WA during summer, based on NCEP/NCAR reanalysis data from 1979 to 2005 [1].

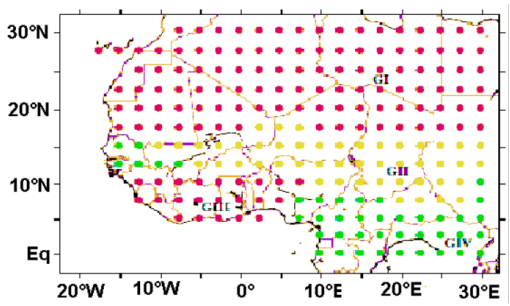

Figure 10. Presentation of the four (GI, GII, GIII, and GIV) analysis regions in WA [39].

As previously mentioned, CCA is performed within the subspace defined by the first few EOFs. Therefore, the analysis of the summer variability of CAPE and CIN is done by using EOF analysis and then the examination of the correlation structure between CAPE, CIN, and rainfall using the CCA method is explored. **Figure 11** shows the two first CCA pairs of CAPE and rainfall from GPCP. This method identifies pairs of CAPE and rainfall patterns that maximize the correlation between their corresponding pattern of the coefficients.

In **Figure 11a**, which highlights the first CCA pair, the correlation coefficient shows variation, decreasing and increasing towards the north. Specifically, in region GIII, the correlation coefficient is approximately 0.7, with a peak around coordinates (8°N, 12°W), and reaches 0.8 in region GIV. In region GI, the correlation coefficient ranges from 0.6 to 0 at 15°N, becoming negative after that and increasing northwards, with a maximum at lat 18°N–23°N and lon 12°E–25°E.

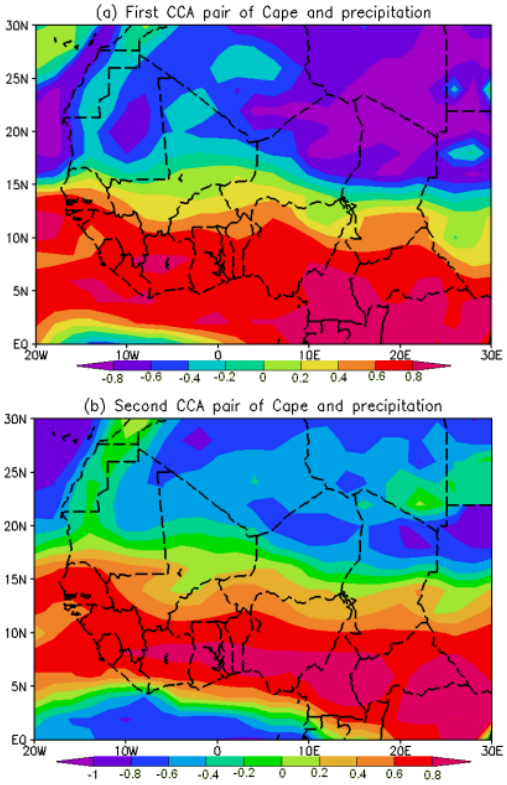

Figure 11. The pairs of CCA of CAPE and rainfall during JJAS 2006 over West Africa. (**a**) first pair and (**b**) second pair .

Figure 12 shows the first two CCA pairs of CIN and rainfall from GPCP (**Figure 12a,b**). The configuration observed for the first two CCA pairs of CAPE and precipitation is similarly found for CIN and precipitation. Specifically, the Guinea Coast (GIII) and the wet Central Africa (GIV) exhibit

greater sensitivity to interannual variability in African wave activity, as noted by Thorncroft and Blackburn [18]. In contrast, the first CCA pairs of CAPE (CIN) and precipitation predominantly characterize the arid and semi-arid regions of the study area. In the first CCA pair of CIN and precipitation, the correlation coefficient is approximately 0.7 in region GI. It decreases northwards from 12°N to zero around 18°N, becoming negative. A similar pattern is found in region GIII **(Figure 12a)**, where the correlation coefficient decreases from 12°N to the equator. In region GIV, the correlation coefficient is around 0.9.

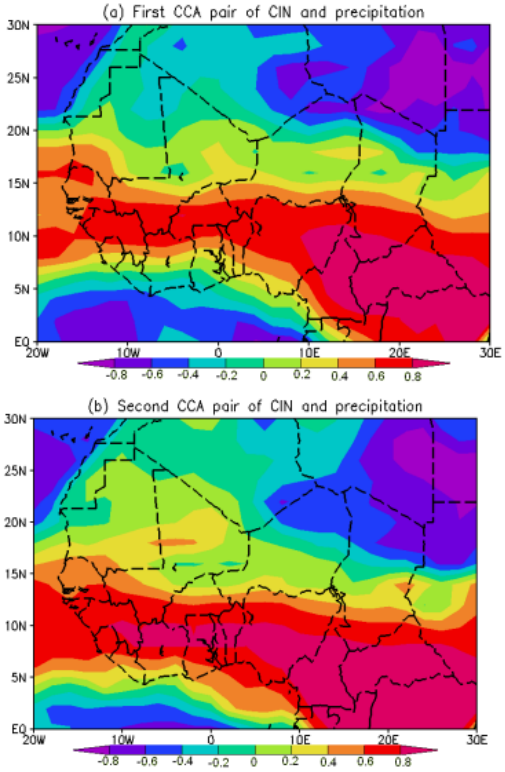

Figure 12. First two pairs of CCA of CIN and precipitation over West Africa for JJAS 2006. (**a**) First pair and (**b**) second pair .

The first pairs of canonical correlations for CAPE and CIN and rainfall identify the positions of the correlation coefficient maxima between CAPE, CIN, and rainfall, which is aligned with ITCZ in WA; underscoring the significant role of the ITCZ in rainfall patterns. The second pairs of CCA for CAPE and rainfall or CIN and rainfall predominantly describe the northern parts of the study area (GIII and GIV). The strong link between patterns in this western part suggests a higher likelihood of intense convection, which is coupled with the importance of stabilizing required stable surface conditions. Thus, the critical correlation coefficient of the first CCA pair is 0.21 at the 95% confidence level and has a correlation of about 68% and 12.2 degrees of freedom. In the arid (GI) and semi-arid (GII) regions, this pair explains about 78% and 73% of the regional variance, respectively. These regions are primarily influenced by the first CCA pair. The Guinea Coast (GIII) and wet equatorial area (GIV) are mainly determined by the second CCA pair, which accounts for more than 60% of the regional variance and has a correlation coefficient is 0.65 with 10.8 degrees of freedom.

4. Conclusions

We used the ERA-Interim dataset over WA from June to September 2006 and applied the Mann-Kendall trend test to estimate and analyze trends in CAPE and CIN. Climatological analyses of CAPE and CIN were conducted using Empirical Orthogonal Functions (EOF), and their relationship with precipitation was explored through Canonical Correlation Analysis (CCA). The climatology includes seasonal means and trends. However CAPE and CIN are derived from similar equations, and their temporal and spatial distributions differ significantly. CAPE values increase towards the ITCZ with decreasing latitude, while CIN peaks between the equator and 30°N, showing a bimodal zonal distribution.

Regarding convection genesis and intensity, an increase/decrease in CAPE/CIN suggests a higher likelihood of more vigorous convection, which may require more significant forcing to overcome the stability of the surface conditions. Thus, we found an increase in CAPE and a decrease in CIN in the summer (JJAS) 2006 over WA, which justifies the lengthening of the observed rainy season. Furthermore, the first three EOFs of CAPE and CIN during this period indicate that we have a variance of about 42% for the first EOF of CAPE and 44% for CIN. We have a variance of 16.4% and 12% for the second EOF respectively for CAPE and CIN. We can also note the strong correlation between CAPE and precipitation as indicated by their PC1 time series. In the same logic, significant correlations are observed between CIN and temperature at the 95% confidence level.

A strong dependence of CAPE and CIN on precipitation is also reflected by the first pair of CCA in West Africa. This strong correlation suggests that during this period there is a greater probability of intense convection and a need for more substantial forcing to overcome the improved stable surface

conditions in this region. The correlation of the first CCA pair is 68% and 12.2 degrees of freedom and has a lower correlation coefficient of 0.21 at the 95% confidence level. In the arid (Sahel) and semi-arid (Sahelo-Sahelian) regions, the first CCA pair explains approximately 78% and 73% of the regional variance, respectively. The Guinea Coast and the wet equatorial areas are primarily influenced by the second CCA pair, which explains more than 60% of the regional variance and has a correlation coefficient of approximately 0.65 with 10.8 degrees of freedom. CAPE and CIN reflect the vertical structure of the lower troposphere in WA and contribute to the study of convection through the CCA method.

Author Contributions

C.M. conceived, analyzed, and interpreted the data used in the study. C.A.M. analyzed the data and reviewed the manuscript. E.E. contributed to revising and formatting the manuscript. S.Z. designed and collected the data used in the study. A.L. contributed to revising and supervised the study. D.M. (Desmond Manatsa) contributed to revising and supervised the study. D.M. (David Monkam) contributed to revising and supervised the study. All authors read and approved the final manuscript.

Funding

This work received no external funding.

Institutional Review Board Statement

Not applicable.

Informed Consent Statement

Not applicable.

Data Availability Statement

Data is available online on the AMMA International Website http://www.amma-international.org.

Acknowledgments

We greatly thank the international scientific group for initiating the AMMA program, as well as the various research institutions from France, the United Kingdom, the United States, and Africa that contributed to the establishment and consolidation of this data collection program (Detailed information on scientific coordination and funding is available online on the AMMA International Website http://www.amma-international.org). We thank LEMAP of the University of Yaoundé I. We also appreciate the comments of the anonymous reviewers which helped to improve the quality of the manuscript.

Conflicts of Interest

The authors declare no conflict of interest.

References

[1] Lenouo, A, Monkam, D, Mkankam, F.Kamga, 2010. Variability of static stability over West Africa during Northern Summer 1979–2005. Atmospheric Research. 98(2–4), 353–362.

[2] Adedokun, J.A., 1982. On an instability index relevant to precipitation forecasting in West Africa. Archives for meteorology, geophysics, and bioclimatology, Series A. 31(3), 221–230.

[3] Rezacova, D., Motl, V., 1990. The use of the simple 1D steady-state convective cloud model in the decision tree for determining the probability of thunderstorm occurrence. Studia Geophysica et Geodaetica. 34(2), 147–166.

[4] Embolo Embolo, G.B., Lenouo, A., Nzeukou, A.T., et al., 2017. On convection and static stability during the AMMA SOP3 campaign. Theoretical and Applied Climatology. 127, 197–211. DOI: https://doi.org/10.1007/s00704-015-1627-3

[5] Sanchez, J.L., Fraile, R., De la Fuente, M.T., Marcos, J.L., 1998. Discriminant analysis applied to the forecasting of thunderstorms. Meteorology and Atmospheric Physics. 68, 187–195.

[6] Rasmussen, E.N., Blanchard, D.O., 1998. A baseline climatology of sounding-derived supercell and tornado forecast parameters. Weather and Forecasting. 13(4), 1148–1164.

[7] Brooks, H.E., Lee, J.W., Craven, J.P., 2003. The spatial distribution of severe thunderstorm and tornado environments from global reanalysis data. Atmospheric Research. 67, 73–94.

[8] Brooks, H.E., Anderson, A.R., Riemann, K., Ebbers, I., Flachs, H., 2007. Climatological aspects of convective parameters from the NCAR/NCEP reanalysis. Atmospheric Research. 83(2–4), 294–305.

[9] Markowski, P.M., Straka, J.M., Rasmussen, E.N., 2002. Direct surface thermo-dynamic observations within

rearflank downdrafts of nontornadic and tornadic supercells. Monthly Weather Review. 130(7), 1692–1721.

[10] Ye, B., Del Genio, A.D., LO, K.K., 1998. CAPE variations in the current climate and in a climate change. Journal of Climate. 11(8), 1997–2015.

[11] Meukaleuni, C., Lenouo, A., Monkam, D., 2015. Climatology of Convective Available Potential Energy (CAPE) in ERA-Interim reanalysis over West Africa. Atmospheric Science Letters. 17(1), 65–70.

[12] Wahiduzzaman, M., Ali, M.A., Luo, J.J., et al., 2022. Effects of convective available potential energy, temperature and humidity on the variability of thunderstorm frequency over Bangladesh. Theoretical And Applied Climatology. 147, 325–346. DOI: https://doi.org/10.1007/s00704-021-03833-4

[13] Lafore, J.P., Flamant, C., Giraud, V., et al., 2010. Introduction to the AMMA Special issue on "Advances in understanding atmospheric processes over West Africa through the AMMA field campaign". Quarterly Journal of the Royal Meteorological Society. 136(SUPP 1), 2–7.

[14] Lafore, J.P., Flamant, C., Guichard, F., et al., 2011. Progress in understanding of weather systems in West Africa. Atmospheric Science Letters. 12(1), 7–12.

[15] Parker, D.J., Thorncroft, C.D., Burton, R.R., Diongue-Niang, A., 2005. Analysis of the African easterly jet, using aircraft observations from the JET2000 experiment. Quarterly Journal of the Royal Meteorological Society. 131(608), 1461–1482.

[16] Burpee, R.W., 1972. The origin and structure of easterly waves in the lower troposphere of North Africa. Journal of the Atmospheric Sciences. 29(1), 77–90.

[17] Cook, K.H., 1999. Generation of the African Easterly Jet and Its Role is Determining West African Precipitation. Journal of Climate. 12(5), 1165–1184.

[18] Thorncroft, C.D., Blackburn, M., 1999. Maintenance of the African easterly jet. Quarterly Journal of the Royal Meteorological Society. 125(555), 763–786.

[19] Thorncroft, C.D., Hoskins, B.J., 1994. An idealized study of African easterly waves. I: A linear view. Quarterly Journal of the Royal Meteorological Society. 120(518), 953–982.

[20] Houze, R.A and Betts A.K., 1981. Convection in GATE. Reviews of Geophysics. 19(4), 541–576.

[21] Mohr, K.I., Thorncroft, C.D., 2006. Intensive convective systems in West Africa and their relationship to the African easterly jet. Quarterly Journal of the Royal Meteorological Society. 132(614), 163–176.

[22] Wu, M.C., Reale, O., Schubert, S.D., et al., 2009. African Easterly Jet: Structure and Maintenance. Journal of Climate. 22(17), 4459–4480.

[23] Laurent, H., Jobard, I., Toma, A., 1998. Validation of satellite and ground-based estimates of precipitation over the Sahel. Atmospheric Research. 47–48, 651–670.

[24] Yano, J.I., Fraedrich, K., Blender, R., 2001. Tropical convective variability as 1/f noise. Journal of Climate. 14(17), 3608–3616.

[25] Parker, D.J., 2002. The response of CAPE and CIN to tropospheric thermal variations. Quarterly Journal of the Royal Meteorological Society. 128(579), 119–130.

[26] Romero, R., Gaya, M., Doswell III, C.A., 2007. European climatology of severe convective storm environmental parameters: a test for significant tornado events. Atmospheric Research. 83(2–4), 389–404.

[27] Trapp, R.J., Diffenbaugh, N.S., Brooks, H.E., et al., 2007. Changes in severe thunderstorm environment frequency during the 21st century caused by anthropogenically enhanced global radiative forcing. Proceedings of the National Academy of Sciences. 104(50), 19719–19723.

[28] Riemann-Campe, K., Blender, R., Friedrich, K., 2011. Global memory analysis in observed and simulated CAPE and CIN. International Journal of Climatology. 31(8), 1099–1107.

[29] Agustí-Panareda, A., Beljaars, A., Cardinali, C., Genkova, I., Thorncroft, C., 2010. Impacts of assimilating AMMA soundings on ECMWF analyses and forecasts. Weather and Forecasting. 25(4), 1142–1160.

[30] Dee, D.P., et al., 2011. The ERA-Interim reanalysis: configuration and performance of the data assimilation system. Quarterly Journal of the Royal Meteorological Society. 137(656), 553–597.

[31] Adler, R.F., Huffman, G.J., Chang, A., et al., 2003. The version 2 Global Precipitation Climatology Project (GPCP) Monthly Precipitation Analysis (1979-Present). Journal of Hydrometeorology. 4(6), 1147–1167.

[32] Huffman, G.J., Adler, R.F., Morrissey, M., et al., 2001. Global Precipitation at One-Degree Daily Resolution from Multi-Satellite Observations. Journal of Hydrometeorology. 2(1), 36–50.

[33] Xie, P., Janowiak, J.E., Arkin, P.A., et al., 2003. GPCP Pentad Precipitation Analyses: An Experimental Dataset Based on Gauge Observations and Satellite Estimates. Journal of Climate. 16(13), 2197–2214.

[34] Wilks, D.S., 2011. Statistical Methods in the Atmospheric Sciences, 3rd ed. Academic Press: Oxford, UK. pp. 561.

[35] Sultan, B., Janicot, S., 2003. The West African monsoon dynamics. Part II: The ''preonset'' and ''onset'' of the summer monsoon. Journal of Climate. 16(21), 3407–3427.

[36] Parker, D.J., Burton, R.R., Diongue-Niang, A., et al., 2005. The diurnal cycle of the west African monsoon circulation. Quarterly Journal of the Royal Meteorological Society. 131(611), 2839–2860.

[37] Ventrice, M.J., Thorncroft, C.D., Schreck III, C.J., 2012. Impacts of Convectively Coupled Kelvin Waves on Environmental Conditions for Atlantic Tropical Cyclogenesis. Monthly Weather Review. 140(7),

2198–2214.

[38] Riemann-Campe, K., Friedrich, K., Lunkeit, F., 2009. Global Climatology of Convective Available Potential energy (CAPE) and Convective Inhibition (CIN) in ERA-40 reanalysis. Atmospheric Research. 93(1–3), 534–545.

[39] Yepdo, D.Z., Monkam, D., Lenouo, A., 2009. Spatial Variability of Rainfall Regions in West Africa during the 20th century. Atmospheric Science Letters. 10(1), 9–13.